TRI-PP-89-23
May 1989

Gamow-Teller Strength Deduced from Charge Exchange Reactions on ^{54}Fe at 300 MeV

M.C. Vetterli[1], O. Häusser[1,2], R. Abegg[2],
W.P. Alford[3], A. Celler[1], D. Frekers[2,4], R. Helmer[3],
R. Henderson[2,5], K.H. Hicks[2], K.P. Jackson[2], R.G. Jeppesen[1]
C.A. Miller[2], K. Raywood[5], S. Yen[2].

1) Simon Fraser University, Burnaby, British Columbia, Canada, V5A 1S6.
2) TRIUMF, 4004 Wesbrook Mall, Vancouver, British Columbia, Canada, V6T 2A3.
3) University of Western Ontario, London, Ontario, Canada, N6A 3K7.
4) University of Toronto, Toronto, Ontario, Canada, M5S 1A7.
5) University of Melbourne, Melbourne, Australia.

ABSTRACT

Angular distributions of the ^{54}Fe(p,n)^{54}Co and ^{54}Fe(n,p)^{54}Mn cross sections have been measured to test the Gamow-Teller sum rule ($S_- - S_+ = 3(N-Z)$) in a case where the GT strength is large for both channels. The results for S_- and S_+ are compared to several models which have moderate success in describing the data. Large scale shell model and quasi-particle RPA calculations correctly predict the distribution of GT strength but overestimate the total strength. A model which approximates the nuclear surface to be a semi-infinite slab describes the cross sections well in the quasi-elastic scattering region if 2p-2h correlations are included.

NUCLEAR REACTIONS: ^{54}Fe(n,p)^{54}Mn, E=298 MeV, angular distribution.
^{54}Fe(p,n)^{54}Co, E=300 MeV, angular distribution.

PACS nos.: 25.40 Ep, 25.40 Fq, 24.30 Cz, 27.40 +z.

I. INTRODUCTION

Nucleon charge exchange reactions change the value of T_3, the third component of isospin and hence involve purely isovector interactions; the isoscalar amplitude which dominates (p,p') reactions is forbidden. This makes (p,n) and (n,p) reactions ideal for studying the isovector part of the N-nucleus interaction.

The most striking feature of 0° (p,n) reactions at low energies ($\leq$100 MeV) is the isobaric analog resonance (IAR) ($T=T_0$, $\Delta S=\Delta L=0$, where T_0 is the isospin of the target) which is related to Fermi (F) β-decay [1]. The IAR corresponds to transitions between analog states in the parent and daughter nuclei. At energies above 100 MeV, the $\sigma\tau$ part of the N-nucleus interaction is larger than the τ component[2] and the Gamow-Teller (GT) resonance ($\Delta T=\Delta S=1$, $\Delta L=0$) dominates the small angle spectra. The study of (p,n) reactions has the advantage over β-decay measurements that the GT strength can be investigated over a large region of excitation energy in the residual nucleus. This has led to extensive studies of intermediate energy (p,n) reactions in recent years [3,4,5]. A reduction in the amount of Gamow-Teller strength is observed relative to theoretical calculations and the GT sum rule, discussed below. This Gamow-Teller quenching is on the order of 30-40%.

The development of a nucleon charge exchange facility at TRIUMF has made possible the study of intermediate energy (n,p) reactions. In all nuclei heavier than ^{3}He, this reaction populates only $T=T_0+1$ states. Other final states (including the IAR) are forbidden and Gamow-Teller transitions can be observed relatively free of background.

This paper presents data for the ^{54}Fe(p,n)^{54}Co and ^{54}Fe(n,p)^{54}Mn reactions at 300 MeV. Results of the latter experiment have been published previously in a letter[6] where the relevance of the (n,p) data to astrophysics is also discussed. Gamow-Teller strength is extracted in both cases and the results are combined to test the GT sum rule. The strength and distribution of the GT transitions are compared also to shell model and quasi-particle RPA calculations. Furthermore, the quasi-elastic region is studied within the framework of a semi infinite slab model. The cross sections for the (n,p) and (p,n) reactions are related to the isovector piece of the (p,p') cross section by isospin coupling coefficients. Hence, the charge exchange data can be used to decompose the (p,p') cross section into its isospin components. This is discussed extensively for ^{54}Fe in ref. 7.

II. EXPERIMENTAL METHOD

The TRIUMF nucleon charge exchange facility is discussed in detail elsewhere [8]. However, a short description is included here for completeness. The setup for (p,n) experiments is shown schematically in fig.1.

1) (p,n) configuration.

A proton beam from the TRIUMF cyclotron strikes the primary target located at the pivot of the Medium Resolution Spectrometer[9] (MRS) on beam line 4B. A

compact sweeping magnet bends the proton beam 20 degrees to the right into a shielded beam dump. The neutrons from the (p,n) reaction continue undeflected by the magnetic field and strike a recoil scintillator (RS) 92 cm downstream of the primary target. The RS is a 2.54 cm x 2.54 cm x 6.0 cm glass vessel filled with BICRON BC513 liquid scintillator. The ratio of hydrogen to carbon is 2:1 and the density is 0.735 g/cm^3, yielding a hydrogen (carbon) target thickness of 0.267 g/cm^2 (1.6 g/cm^2). Recoil protons emitted near 0° in the ^{1}H(n,p) reaction are analyzed by the MRS. The conversion efficiency of the RS is about 1.7x10^{-5} for an MRS solid angle of 2 msr. The amplitude of the signal from the scintillator is used to correct the momentum of the proton detected in the spectrometer for energy loss in the RS. This technique allows the use of a thick neutron converter without sacrificing energy resolution. In this experiment, the observed resolution was 1.8 MeV with a tightly focussed achromatic beam and about 1.2 MeV with a momentum dispersed beam incident on a 7 mm wide strip target. The primary targets were ^{7}Li (110 mg/cm^2) and ^{54}Fe (139.3 mg/cm^2).

Although the sweeping magnet deflects most of the protons from the recoil scintillator, the background from charged particles is still significant. A tungsten alloy blocker placed on the left side of the beam between the target and the RS prevents protons scattered to this side from being bent into the recoil scintillator by the sweeping dipole. At angles larger than 5°, the blocker is not sufficient and some extra absorber consisting of 8.5 cm of copper and 0.3 cm of lead was added at the exit of the magnet. A thin plastic scintillator in front of the RS is used to veto the remaining charged particles.

Two front end chambers (FECs) at the entrance to the MRS are used to raytrace back to the RS. Software gates are used in both the horizontal and vertical directions to reduce the background from scattered beam particles or neutrons converting outside the recoil scintillator. The efficiency of the MRS wire chambers was determined by the redundancy of planes in each detector. The dead time was measured by pulser pseudo-events. The ratio of pulser events detected to events generated measures the live time of the system. The beam was integrated using the beam dump as a Faraday cup. A small reverse leakage current was monitored and remained relatively constant throughout the experiment ($I_R \approx$ (–2.5 to –4.0 nA) compared to $I_{BEAM} \approx$ 200nA).

2) (n,p) configuration.

For (n,p) experiments, the sweeping dipole is moved upstream such that the secondary target is at the pivot of the MRS. The ^{7}Li(p,n)^{7}Be reaction is used to produce a nearly monoenergetic beam of neutrons. This reaction populates the ground state and the unresolved 429 keV state in ^{7}Be; this contributes to the energy spread of the neutron beam. Furthermore, a long continuum tail is produced which amounts to about 1% of the peak area per MeV. A method of obtaining the neutron line shape for deconvolution from the (n,p) spectra is outlined below. The neutron flux at the (n,p) targets is about 4.10^4 /sec/cm^2 for a dispersed beam intensity of 150 nA and a 110 mg/cm^2 thick ^{7}Li target.

The secondary (n,p) target box consists of six target layers separated by proportional wire chambers[10]. A thin scintillator just upstream of the target box vetoes charged particles. The first wire chamber consists of a double plane both of which also act as vetos. Although the blocker in the sweeping dipole is present in both configurations, the extra absorber needed for (p,n) experiments at large angles is not used for (n,p) experiments. The target arrangement was: empty, ^{12}C (46 mg/cm^2), empty, two ^{54}Fe (140 mg/cm^2 each), and CH_2 (47.2 mg/cm^2). The pattern of hit wires in the target box allows one to determine in which of the six layers the (n,p) reaction took place. Corrections are made for energy loss in the subsequent targets and good resolution ($\approx$ 1 MeV) can be recovered. Furthermore, the layered arrangement allows the use of a target of known cross section (usually CH_2) in one of the positions to normalize the data independent of beam current, dead time, and MRS efficiency.

A good efficiency is required for the target wire planes to reduce the occurrence of target mis-identification. These efficiencies are determined by placing a thick block of CH_2 upstream of the veto scintillator to convert neutrons into protons. Requiring the veto paddle in the trigger ensures that only protons entering the box are considered. For 100% target box efficiency, there should be hits in all planes for each event, and hence the number of misses in each plane is a measure of the inefficiency of that detector layer. Inefficiencies on the order of 1-2% were observed. Corrections for these are described below.

Since this was one of two commissioning experiments for the CHARGEX facility, several gases were used in the target box. Isobutane, the usual FEC gas, was first used but then abandoned because of the large contribution to the spectra from hydrogen (half the yield at E_x=0 MeV). A 90%-10% mixture of Argon-CO_2 was determined to be the best and has been used in all charge exchange experiments since. Contributions from the different gas mixtures are shown in ref. 10.

The two FECs are again used to raytrace back to the target. In order to reduce the number of multiple hits in a target plane resulting in the event being rejected in the analysis, software gates on each plane are dynamically set for each event using the traced back position from the FECs. Only the two wires in the vicinity of the traceback are considered for a particular event.

III. RESULTS

1) (p,n).

Data were obtained at 0.9°, 2.5°, 5.0°, 8.0°, 12.0°, and 15° for a beam energy of 300 MeV. Spectra for the cross section versus E_x, the excitation energy in ^{54}Co, are shown in fig.2. The two prominent peaks at 1 MeV and 10 MeV have angular distributions consistent with L=0 transfer. They are identified as Gamow-Teller transitions. This is discussed below. The cross sections were normalized to the summed cross section for transitions to the ground and first excited states in the ^{7}Li(p,n)^{7}Be reaction. This cross section was determined at 0° between 200 MeV

and 400 MeV by Watson *et al* [11] who integrated the angular distribution at each energy and normalized it to the activation analysis of D'Auria *et al* [12]. It was found that a 0° cross section in the laboratory frame of 35±3 mb/sr is consistent with all data between 50 MeV and 400 MeV. Several measurements of the ^{7}Li(p,n)^{7}Be yield were included during the present experiment and were reproducible within 1%. This consistency provides confidence that the efficiency and the dead time of the MRS system, as well as the beam integration were determined reliably by the experiment. The different runs were normalized to each other taking into account these three factors.

As mentioned above, a strip target with dispersed beam was used to improve the energy resolution. Measurements were also done with an achromatic beam at each angle. In this case, all of the primary beam hits the target and these data are used to normalize the cross sections with respect to ^{7}Li(p,n). Both achromatic and dispersed spectra were integrated over the entire range of excitation energy and a normalization factor, which represents the fraction of the beam hitting the target for the dispersed beam, was determined for each angle. Furthermore, for angles greater than 5°, a correction was applied for the extra absorber placed at the exit of the sweeping dipole. Measurements were done both with and without absorber at 5°. An absorption factor of 1.92 was used to correct the cross sections at 8°, 12°, and 15°.

Finally, the spectra have to be corrected for (n,p) reactions with the carbon in the recoil scintillator. A spectrum for the ^{12}C(n,p)^{12}B reaction (Q-value=−12.6 MeV) was obtained during the (n,p) phase of the experiment. The ^{7}Li(p,n)^{7}Be spectrum shows a clear peak at E_x=12.6 MeV. This peak is a satellite of the (ground state, first excited state) peak at $E_x \approx 0$ MeV and arises from the carbon in the RS. The ^{12}C(n,p) spectrum is normalized to this peak and the resolution of the two experiments is matched by smearing the (n,p) data. The ^{12}C(n,p) spectrum is then deconvoluted from the (p,n) spectrum. The result of this procedure is shown in fig.3. The spectra of fig.2 are corrected for all the effects mentioned above.

2) (n,p).

Data were taken at 1.8°, 2.9°, 5.4°, 8.3°, and 12° for a beam energy of 298 MeV. Corrections were made for the difference in neutron flux and MRS solid angle for each individual target layer, as well as for the acceptance of the spectrometer as a function of excitation energy. The results for the cross section versus the excitation energy in ^{54}Mn are shown in fig.4. The peak at $E_x \approx 2$ MeV is consistent with an L=0 angular distribution and is identified as the GT resonance. A broad peak at $E_x \approx 12$ MeV appears at 5.4°. Its angular distribution agrees with an L=1 shape characteristic of a dipole resonance. As mentioned above, the experiment is self-normalizing. A CH_2 target was included in the target stack and the cross sections were normalized relative to the ^{1}H(n,p) reaction. A value of 50.7 mb/sr in the laboratory frame was used for this cross section at 1.8°. This is the average effective scattering angle in the laboratory frame with the MRS at 0°. It arises from the solid angle subtended by the secondary (n,p) targets with respect to the

primary (p,n) target and the acceptance of the MRS. The value of the cross section was taken from a phase shift analysis of N-N data [13].

One of the major concerns with the secondary target box is the problem of target mis-identification. This happens mostly when a proton from one target is identified as coming from the target immediately downstream of it due to an inefficiency in the wire plane separating them (target leak through). For example, an (n,p) reaction occurring in the third target is tagged by no hits in the first three wire chambers and one hit in each of the four downstream planes. An inefficiency in the detector layer immediately following target 3 will result in the following hit pattern: 4 misses, 3 hits. This mistakenly signals an (n,p) reaction in the fourth target. This effect is corrected by subtracting from the downstream spectrum a certain fraction of the upstream spectrum determined from the measured inefficiencies of the target wire planes (see section II). Because of this effect, targets with large yields, such as CH_2 are placed in the last position of the stack.

Since the targets are interspersed with proportional wire chambers, a small contribution to the spectra arises from the detector gas and windows. This is corrected by the subtraction of spectra recorded without the (n,p) targets present (target "empty" runs).

As mentioned above, the ^{7}Li(p,n)^{7}Be reaction does not produce strictly monoenergetic neutrons and the tail of the distribution must be deconvoluted from the data. The shape of the neutron spectrum is determined by comparing the yields from CH_2 and carbon targets in the secondary position. By subtracting the latter spectrum from the former after correction for target thickness, the spectrum for ^{1}H(n,p) is obtained. This spectrum, plotted in fig.5, is assumed to reflect the energy distribution of the incident neutron beam. Note that this is the same as the carbon corrected ^{7}Li(p,n)^{7}Be spectrum of fig.3 since these are measurements of the same double scattering process using the two different modes of the CHARGEX configuration.

IV. MULTIPOLE DECOMPOSITION

In order to extract strengths for the different giant resonances, in particular the Gamow-Teller strength, a multipole decomposition of the cross sections was done. The data were summed into 1 MeV wide bins and angular distributions were generated for each one. Theoretical angular distributions for each angular momentum transfer were calculated using the distorted wave impulse approximation (program DW81 [15]) with the Franey-Love interaction [16] at 270 MeV. The optical potentials used for the distortions in DW81 were phenomenological Woods-Saxon potentials fit to elastic scattering data taken at TRIUMF [7]. The following simple shell model configurations relative to a ^{56}Ni core were assumed for the final states of the (n,p) reaction (initial state: $\pi(f_{7/2})^{-2}$):

$$\Delta L = 0 : [\pi(f_{7/2})^{-3}, \nu(f_{5/2})]_{1^+}$$
$$\Delta L = 1 : [\pi(f_{7/2})^{-3}, \nu(g_{9/2})]_{1^-}$$

$$\Delta L = 2 : [\pi(f_{7/2})^{-3}, \nu(f_{5/2})]_{3^+}.$$

The variation in the ΔL=2 angular distributions for the different J^{π}_{final} is small and the choice of the configuration is unimportant in this case. However, the shapes for ΔL=1 (J^{π}= 0^-, 1^-, 2^-) vary somewhat depending on J^{π}_{final}. Without a detailed shell model calculation, it is difficult to know how to combine the three shapes. The simplest procedure is to choose one. This, together with the approximation of single particle states, will introduce a systematic error in the multipole decomposition which is difficult to estimate. It should be noted that the fitting procedure will lump all $\Delta L \geq 2$ strength into the ΔL=2 shape. The Q-value dependence of the theoretical angular distributions is taken into account by doing the calculations from E_x= 0 MeV to 40 MeV in 10 MeV steps and interpolating in between. Calculations of the angular distributions for the (p,n) reaction were also done. The shapes were essentially the same as for the (n,p) case. However, one must take into account the shift in excitation energy due to the different Q-values of the reactions (Q(n,p)=0.088 MeV, Q(p,n)=–9.033 MeV).

The angular distribution for each energy bin was fitted independently with a computer program which uses the MINUIT minimization routines. This procedure is described in ref. 17 and is the subject of a future publication. Typical (n,p) angular distributions are shown in fig.6. The three plots are for excitation energy bins where each of the three shapes (ΔL=0,1,2) dominate. Fig.7 shows the fitted coefficients for ΔL=0 which, although determined independently for each bin, vary smoothly with excitation energy. This gives confidence in the multipole decomposition procedure. Since this is a plot of the fitting coefficients, the units are arbitrary. The coefficients must be multiplied by the appropriate DWIA cross sections at each angle to get the fitted cross section. This is done in fig.8 for the 1.8° (n,p) data and in fig.9 for the 0.9° (p,n) data.

V. σ/B(GT) CALIBRATION

It can be shown in the Distorted Wave Impulse Approximation (DWIA) that the 0° (p,n) cross section is proportional to B(GT)[3,5], where

$$B(GT^{\pm}) = \frac{|<f||\sigma t^{\pm}||i>|^2}{2j_i+1}$$

The proportionality constant can be determined by measuring the 0° (p,n) cross section in a case where the β-decay is known. Alternately, a theoretical value for the ratio σ/B(GT) can be calculated using a computer code such as DW81 for the cross section. The latter method was used for the (n,p) study of ref. 6. In the case of ^{54}Fe(p,n) however, it is possible to determine σ/B(GT) experimentally from the state at 0.94 MeV in ^{54}Co. The value of B(GT) for this state is deduced from previous (p,n) experiments at 160 MeV [14] and 135 MeV [18] where the cross section was measured and an average σ/B(GT) for this mass region and the appropriate incident energy was used to calculate B(GT). They found: B(GT)=0.73 ± 0.10. Although the resolution for the present experiment does not permit the separation of the 0.94 MeV state and the ground state (IAR), this pair can be distinguished

from the rest of the spectrum. The fraction of the peak attributable to the 0.94 MeV state can be determined from the following equation[5] if it is assumed that all of the Fermi strength is in the ground state transition (B(F)=2):

$$f_{GT} = 1 - f_F = \left[1 + \frac{B(F)}{B(GT)R^2}\right]^{-1}$$

where

$$R = \frac{J_{\sigma\tau}}{J_{\tau}}\sqrt{\frac{N_{\sigma\tau}}{N_{\tau}}}.$$

$J_{\sigma\tau}$ and J_{τ} are the volume integrals of the $\sigma\tau$ and τ parts of the N-N interaction and $N_{\sigma\tau}$ and N_{τ} are distortion factors. The ratio R^2 was measured by Alford *et al*[2] between 200 MeV and 450 MeV. The value at 300 MeV is 14.6±1.0. One obtains f_{GT}= 0.84 and therefore f_F= 0.16. The cross section for the peak is 4.63±0.21 mb/sr. Correcting for the center-of-mass, the ground state, and the effective scattering angle, we get: $\sigma_{CM}(0°)$= 3.66±0.24 mb/sr and hence:

$$\sigma_{CM}/B(GT)(0°, \omega = 11 MeV) = 5.0 \pm 0.75 mb/sr,$$

where ω is the energy transfer (ω= E_x - Q). Using DW81 to extrapolate to ω=0, we get:

$$\hat{\sigma} \equiv \sigma_{CM}/B(GT)(q = \omega = 0) = 5.1 \pm 0.8 mb/sr,$$

where q is the momentum transfer. This compares to $\hat{\sigma} \approx$ 5.75±0.8 at 160 MeV[14]. One does not expect a rapid variation in σ/B(GT) with energy because the $\sigma\tau$ interaction is fairly constant in this energy range. Furthermore, the total N-N interaction is also flat in this region and hence the distortions should be somewhat energy independent. The value of 3.4 for σ/B(GT) which was calculated in ref.6 using DW81 and the Franey-Love interaction does not agree with experiment. The effect of this on the Gamow-Teller strength in (n,p) deduced in ref.6 is discussed below.

VI. GAMOW-TELLER STRENGTH

1) Results.

The 0°, ΔL=0, (n,p) cross section was integrated up to E_x=10 MeV. The strength above this excitation energy was not included because of uncertainties in the fitting procedure for small components of the cross section. In particular, a small change in the ΔL=1 shape at small angles will affect the ΔL=0 strength in the region where the ΔL=1 dominates. The uncertainty in the determination of the ΔL=0 component below E_x=10 MeV is estimated to be ±5%. This does not include any systematic error introduced by ignoring the ΔL=0 strength above 10 MeV.

The center-of-mass cross sections are given in 2 MeV bins in the second column of table I. The uncertainties include ±5% for the normalization with respect to H(n,p). Since the multipole decomposition was done every 1 MeV, the ΔL=0

component can be determined for each bin (3rd column). As mentioned above, a further ±5% uncertainty in the ΔL=0 fraction was included. Corrections for the effective scattering angle and the energy transfer determined from the DWIA are made for the ΔL=0 component in column 4. A value of $\sigma/B(GT)$= 5.1±0.8 was used to calculate the β-decay strengths B(GT$^+$) in the final column. The integrated strength below 10 MeV in excitation is:

$$B(GT^+) = 3.1 \pm 0.6.$$

The 0° (p,n) cross section was summed up to E_x=15 MeV. The same criteria as for (n,p) were used to decide the upper limit of the integration. The results are shown in table II where the columns are the same as for table I. Note that the effective scattering angle for (p,n) is smaller (θ_{eff}= 0.9°) than for (n,p) since it depends only on the solid angle subtended by the recoil scintillator at the primary target. Note also that the cross sections are corrected to θ= 0° and ω= 11 MeV, the position of the 0.94 MeV state, not q=ω=0. Therefore, the value of $\sigma/B(GT)$ used was 5.0±0.75 mb/sr. The cross sections for the first three energy intervals were summed in the table in order to subtract the contribution from the ground state which is not GT. This was determined in section V to be 16% of the peak or 0.7±0.05 mb/sr. The integrated strength below 15 MeV is:

$$B(GT^-) = 7.5 \pm 1.2.$$

This compares well to the results of Rapaport *et al* [14] who measured the ^{54}Fe(p,n)^{54}Co cross section at 160 MeV and deduced B(GT$^-$)=7.8±1.9. Anderson *et al* [18] have also studied this reaction at 135 MeV and find B(GT$^-$)= 7.0±0.4 below 14 MeV of excitation, in good agreement with the present value.

2) Comparison to theory.

Shell model calculations have been done for B(GT$^+$) by Bloom and Fuller [19] and by Muto [20]. The simplest configuration ($\pi[f_{7/2}]^{-2}$ to $\pi[f_{7/2}]^{-3}\nu[f_{5/2}]$) gives B(GT$^+$)=10.29. Including 1p-1h excitations in both the parent and daughter nuclei reduces B(GT$^+$) to 9.12. The distribution of this strength is plotted in fig.4 as the dashed curve in the top panel. Although the distribution is well reproduced, the calculations must be re-normalized by a factor of 0.34. Expanding the shell model basis to include 2p-2h excitations in ^{54}Fe and using the sum rule technique, Muto finds B(GT$^+$)=7.4, still a factor of 2.4 too large.

It is clear that the inclusion of higher order configurations will reduce the theoretical prediction of B(GT$^+$). However, these calculations quickly become prohibitively large. Auerbach *et al* [21] have done RPA calculations for ^{60}Ni and have shown that RPA correlations reduce the value of B(GT$^+$) by a factor of 2 with respect to the simple shell model. If this same factor applies to ^{54}Fe, we can expect an RPA prediction of B(GT$^+$)=5.15. This gives a quenching factor (σ_{exp}/σ_{th}) of 0.60.

Engel, Vogel, and Zirnbauer (EVZ) have recently performed quasi-particle RPA calculations in an effort to obtain double β-decay matrix elements [22]. Their results for ^{54}Fe [23] are shown in fig.10 where the β-decay strength is plotted with the ΔL=0 component of both cross sections. The distribution of strength is reproduced well as

was the case for the shell model calculations. The total strength predicted by this model is B(GT$^-$)=11.0 and B(GT$^+$)=5.03. Note that the B(GT$^+$) value is consistent with the RPA quenching obtained by Auerbach in ^{60}Ni. The quenching factors with respect to experiment for the RPA model are 0.68 and 0.62 for B(GT$^-$) and B(GT$^+$) respectively. The RPA calculations would agree with the data if the axial vector coupling constant was renormalized in nuclei to g_A/g_V= 1.0. EVZ point out that particle-particle correlations play an important role in the quenching of B(GT). Kuzmin and Soloviev report the same effect in ref. 24 where they find B(GT$^+$)= 4.2. The difference between this and the EVZ value for B(GT$^+$) can probably be attributed to variations in the strength of the particle-particle interaction used.

3) Sum rule.

The σt_- [σt_+] operator is responsible for (p,n) [(n,p)] transitions. If S_- and S_+ are the summed GT strengths for (p,n) and (n,p) reactions, one can write:

$$S_- - S_+ = \sum_{j=1}^{3}\sum_f |\langle f|\sigma_j t_-|i\rangle|^2 - \sum_{j=1}^{3}\sum_{f'} |\langle f'|\sigma_j t_+|i\rangle|^2$$

where $|i\rangle$ and $\langle f|$ are the initial and final states respectively. The σ_j are the Pauli spin matrices and the t's are one half times the corresponding isospin matrices τ_j. Expanding both squares, we get:

$$S_- - S_+ = \sum_{j=1}^{3}\sum_f \langle i|t_-^\dagger\sigma_j^\dagger|f\rangle\langle f|\sigma_j t_-|i\rangle - \sum_{j=1}^{3}\sum_{f'}\langle i|t_+^\dagger\sigma_j^\dagger|f'\rangle\langle f'|\sigma_j t_+|i\rangle.$$

Using closure and the fact that $\sigma_j^\dagger = \sigma_j$:

$$S_- - S_+ = \sum_{j=1}^{3}[\langle i|\sigma_j^2 t_-^\dagger t_-|i\rangle - \langle i|\sigma_j^2 t_+^\dagger t_+|i\rangle].$$

Since σ_j^2= 1, we can sum over j and obtain:

$$S_- - S_+ = 3\langle i|t_-^\dagger t_- - t_+^\dagger t_+|i\rangle.$$

Using the definitions of the isospin raising and lowering operators and the commutation relations for the isospin matrices, one can show:

$$t_-^\dagger t_- - t_+^\dagger t_+ = t_+ t_- - t_- t_+ = [t_+, t_-] = 2t_3.$$

Therefore the above equation simplifies to:

$$S_- - S_+ = 3\langle i|2t_3|i\rangle.$$

A sum over all particles in the nucleus is implicit in the previous discussion. The t_3 operator acting on the neutrons (protons) gives N/2 (-Z/2). We finally obtain:

$$S_- - S_+ = 3(N - Z)$$

This is the well known Gamow-Teller sum rule which has been invoked many times in studies of intermediate energy charge exchange reactions. In particular, since most nuclei have a neutron excess, the proton to neutron transition in the nucleus for (n,p) reactions is Pauli blocked to first order and S_+=0. The sum rule reduces to:

$$S_- \geq 3(N - Z)$$

Intermediate energy (p,n) reactions have shown that S_- is only about 60% of 3(N–Z). This is the Gamow-Teller quenching problem which has received much attention in the past few years. Explanations for the missing cross section range from the strength being shifted to higher energy by 2p-2h admixtures [25] to the excitation of the Δ resonance [26].

^{54}Fe (N–Z=2) was chosen to study the sum rule in a case where both components are large. Using our results for S_- and S_+, we get:

$$S_- - S_+ = (7.5 \pm 1.2) - (3.1 \pm 0.6) = 4.4 \pm 1.3$$

This result is consistent with the ≈40% quenching seen in (p,n) reactions where the (n,p) strength is strongly Pauli blocked. It is difficult to draw definite conclusions because of the large uncertainties. These arise mainly from the multipole decomposition and the determination of the ΔL=0 component of the cross section and the uncertainty in σ/B(GT) . Hence a cross section measurement alone might not reduce the uncertainties enough to sufficiently constrain the results for the sum rule.

VI. QUASI-ELASTIC SCATTERING

We now consider the region of large momentum and energy transfer which is dominated by a broad peak which corresponds to quasi-elastic scattering. In this process the projectile interacts with one of the target nucleons knocking it out of the nucleus. This is similar to N-N scattering except that the interaction takes place in the nucleus. Hence, this is a favorable case to study how the N-N interaction is modified by the nuclear medium. At these excitation energies, discrete nuclear structure has disappeared and the gross features of the response are studied. The model to which we compare the data approximates the nucleus as a semi-infinite slab of nuclear matter, a good approximation since the reaction is surface peaked. This model was originated by Bertsch, Esbensen, and Scholten [27]. The cross section is factorized as:

$$\frac{d^2\sigma}{d\Omega dE} = \sum_{T,S} \left[\frac{k}{k_0} \left(\frac{d^2\sigma}{d\Omega dE} \right)_{NN} N_{eff} \; S_{T,S}(q,\omega) \right]$$

where the k's are wave numbers, $\left(\frac{d^2\sigma}{d\Omega dE}\right)_{NN}$ is the nucleon-nucleon cross section, N_{eff} is the effective number of target nucleons, and $S_{T,S}(q,\omega)$ is the nuclear response. The

model has been modified by Smith[28] and Wambach to include two-step processes and 2 particle - 2 hole (2p-2h) correlations. The effect of the former is not important at excitation energies below 45 MeV [29]. The coupling of 1p-1h RPA excitations used to calculate $S_{T,S}(q,\omega)$ with 2p-2h or higher configurations through the residual interaction shifts strength to higher excitation energy [30]. This is shown in fig.11 for ^{54}Fe(n,p) and fig.12 for ^{54}Fe(p,n). The dashed curve is Smith's calculation for the free nuclear response. The dotted curve is the result of the 1p-1h RPA, while the full curve includes 2p-2h correlations. The (n,p) data are reproduced by the full calculation. Although the prediction is not as good in the (p,n) case, the inclusion of 2p-2h does improve the agreement with the data, notably for the width of the quasi-elastic peak. The absolute normalization of the predictions depends on N_{eff} which is calculated from the elastic scattering data [7].

VII. CONCLUSIONS

In conclusion, the ^{54}Fe(p,n)^{54}Co and ^{54}Fe(n,p)^{54}Mn cross sections have been measured in an effort to study the Gamow-Teller sum rule in a case where S_+ is large. The results are consistent with previous tests of the sum rule using (p,n) reactions on nuclei where the (n,p) strength is strongly suppressed by Pauli blocking. A definitive test of the sum rule is made difficult by the need to determine the ΔL=0 fraction of the cross section, notably at high excitation energy where other multipoles dominate.

Calculations show that the predicted GT strength is reduced as the number of shell model configurations is increased. Although the distribution of strength is reproduced by a simple shell model, all shell model calculations grossly over-estimate the B(GT) strength. RPA calculations which include particle-particle correlations further reduce the total strength and agree with the data if the axial vector coupling constant is renormalized in nuclei such that g_A/g_V= 1.0.

At somewhat larger momentum transfers, calculations of the continuum cross section based on the semi-infinite slab model do reasonably well in the region of the quasi-elastic peak. The inclusion of 2p-2h correlations redistributes strength to higher excitation energy to yield better agreement with the data.

The authors thank G. Fuller and S. Bloom for their shell model calculations and J. Engel for the quasi-particle RPA results. We would also like to thank R.D. Smith for providing the surface RPA calculations and B. Anderson for his (p,n) data. This work was funded by the Natural Sciences and Engineering Research Council of Canada.

REFERENCES

1. J.D. Anderson and C. Wong, Phys. Rev. Lett. 7, 250 (1961).

2. W.P. Alford, R.L. Helmer, R. Abegg, A. Celler, O. Häusser, K. Hicks, K.P.

Jackson, C.A. Miller, S. Yen, R.E. Azuma, D. Frekers, R.S. Henderson, H. Baer, and C.D. Zafiratos, Phys. Lett. B179, 20 (1986).

3. C.D. Goodman, C.A. Goulding, M.B. Greenfield, J. Rapaport, D.E. Bainum, C.C. Foster, W.G. Love, and F. Petrovich, Phys. Rev. Lett 44, 1755 (1980).

4. C. Gaarde, Nucl. Phys. A396, 127c (1983).

5. T.N. Taddeucci, C.A. Goulding, T.A. Carey, R.C. Byrd, C.D. Goodman, C. Gaarde, J. Larsen, D. Horen, J. Rapaport, and E. Sugarbaker, Nucl. Phys. A469, 125 (1987).

6. M.C. Vetterli, O. Häusser, W.P. Alford, D. Frekers, R. Helmer, R. Henderson, K. Hicks, K.P. Jackson, R.G. Jeppesen, C.A. Miller, M.A. Moinester, K. Raywood, and S. Yen, Phys. Rev. Lett. 59, 439 (1987).

7. O. Häusser *et al*, to be published, and M.C. Vetterli, Conf. on the Intersections of Part. and Nucl. Phys., Rockport, Maine, AIP Conference Proceedings 176, ed. G.N. Bunce (1988).

8. R. Helmer, Can. J. Phys. 65, 588 (1987).

9. MRS manual, TRIUMF, unpublished.

10. R.S. Henderson, W.P. Alford, D. Frekers, O. Häusser, R.L. Helmer, K.H. Hicks, K.P. Jackson, C.A. Miller, M.C. Vetterli, and S. Yen, Nucl. Inst. Meth. A257, 97 (1987).

11. J.W. Watson, W.P. Alford, R. Helmer, C. Zafiratos, R. Abegg, A. Celler, S. Elkateb, D. Frekers, O. Häusser, R. Henderson, K. Hicks, K.P. Jackson, R. Jeppesen, C.A. Miller, M. Vetterli, and S. Yen, Bull. Am. Phys. Soc. 32, 1578 (1987).

12. J. D'Auria, M. Domsky, L. Moritz, T. Ruth, G. Sheffer, T.E. Ward, C.C. Foster, J.W. Watson, B.D. Anderson, and J. Rapaport, Phys. Rev. C30, 1999 (1984).

13. R.A. Arndt and L.D. Soper, "Scattering Analysis Interactive Dial-in" (SAID) program, 1984, unpublished.

14. J. Rapaport, T. Taddeucci, T.P. Welch, C. Gaarde, J. Larsen, D.J. Horen, E. Sugarbaker, P. Koncz, C.C. Foster, C.D. Goodman, C.A. Goulding, and T. Masterson, Nucl. Phys. A410, 371 (1983).

15. Computer code DW81, Arizona State University, J.R. Comfort.

16. M.A. Franey and W.G. Love, Phys. Rev. C31, 488 (1985).

17. M.A. Moinester, Can. J. Phys. 65, 660 (1987).

18. B. Anderson, private communication.

19. S.D. Bloom and G.M. Fuller, Nucl. Phys. A440, 511 (1985).

20. K. Muto, Nucl. Phys. A451, 481 (1986).

21. N. Auerbach, L. Zamick, and A. Klein, Phys. Lett. B118, 256 (1982).

22. J. Engel, P. Vogel, and M.R. Zirnbauer, Phys. Rev. C37, 731 (1988).

23. J. Engel, private communication.

24. V.A. Kuzmin and V.G. Soloviev, Nucl. Phys. A486, 118 (1988).

25. G.F. Bertsch and I. Hamamoto, Phys. Rev. C26, 1323 (1982).

26. E. Oset and M. Rho, Phys. Rev. Lett. 42, 47 (1979), and M. Rho, Ann. Rev. Nucl. Part. Sci. 34, 531 (1984).

27. H. Esbensen and G.F. Bertsch, Phys. Rev. C34, 1419 (1986).

28. R.D. Smith, in "Proceedings of the International Conference on Spin Observables of Nuclear Probes", Telluride, Co, 1988, to be published.

29. R.D. Smith and J. Wambach, Phys. Rev. C36, 2704 (1987).

30. R.D. Smith and J. Wambach, to be published in Phys. Rev. C.

TABLE CAPTIONS

Table I. Cross sections and Gamow-Teller strength for the ^{54}Fe(n,p)^{54}Mn reaction at 300 MeV. See the text for an explanation of the different columns.

Table II. Cross sections and Gamow-Teller strength for the ^{54}Fe(p,n)^{54}Co reaction at 300 MeV. See the text for an explanation of the different columns. The strength due to the g.s. transition which is of the Fermi type is subtracted in the fourth line.

TABLE I.

E_x (MeV)	$\sigma_{CM}(1.8°)$ (mb/sr)	$\sigma_{L=0}(1.8°)$ (mb/sr)	$\sigma_{q=\omega=0}$ (mb/sr)	B(GT$^+$)
-1.0	0.21±0.15	0.19±0.14	0.24±0.17	0.05±0.04
1.0	5.36±0.32	5.15±0.40	6.40±0.50	1.26±0.22
3.0	3.78±0.22	3.46±0.27	4.40±0.34	0.86±0.15
5.0	2.86±0.18	2.19±0.17	2.86±0.23	0.56±0.10
7.0	1.78±0.13	0.93±0.08	1.25±0.11	0.25±0.04
9.0	2.00±0.14	0.39±0.03	0.54±0.05	0.11±0.02
				3.09±0.57

TABLE II.

E_x (MeV)	$\sigma_{CM}(0.9°)$ (mb/sr)	$\sigma_{L=0}(0.9°)$ (mb/sr)	$\sigma_{\theta=0,\omega=11}$ (mb/sr)	B(GT$^-$)
-3.0	0.05±0.01	0.05±0.01	0.05±0.01	
-1.0	0.78±0.04	0.78±0.06	0.82±0.06	
1.0	3.11±0.16	3.09±0.22	3.25±0.24	
		minus Fermi:	-0.70±0.24	
			3.42±0.30	0.69±0.12
3.0	1.67±0.09	1.51±0.11	1.62±0.12	0.32±0.05
5.0	3.17±0.17	2.92±0.21	3.19±0.23	0.64±0.10
7.0	4.75±0.24	4.42±0.31	4.93±0.35	0.99±0.16
9.0	10.01±0.51	9.65±0.69	11.07±0.79	2.21±0.36
11.0	8.40±0.43	7.71±0.55	9.15±0.65	1.83±0.30
13.0	3.90±0.20	2.70±0.19	3.32±0.24	0.66±0.10
14.5	1.45±0.08	0.62±0.05	0.76±0.06	0.15±0.03
				7.49±1.22

FIGURE CAPTIONS

Fig.1. CHARGEX facility at TRIUMF in the (p,n) mode. The proton beam strikes the primary target and is bent 20° to the right into a shielded beam dump. The neutrons from the (p,n) reaction are converted to protons by (n,p) reactions in a recoil scintillator (CH_2). The forward going protons are detected in the MRS. Two front end wire chambers are used to trace back to the recoil scintillator to reduce background.

Fig.2. ^{54}Fe(p,n)^{54}Co cross section at six angles between 0.9° and 15°. The peaks at 1 MeV and 10 MeV have a ΔL=0 angular distribution characteristic of Gamow-Teller resonances. The 1 MeV peak includes an unresolved contribution from the Isobaric Analog Resonance.

Fig.3. Deconvolution of the carbon response from the recoil scintillator. a) uncorrected ^{7}Li(p,n) spectrum. The peak at 12.6 MeV is due to the carbon content of the RS. b) corrected spectrum with the effect of the carbon deconvoluted. c) difference between a) and b) which is related to the ^{12}C(n,p) spectrum.

Fig.4. ^{54}Fe(n,p)^{54}Mn cross section at five angles between 1.8° and 12°. The peak at E_x ≈2 MeV is the Gamow-Teller resonance. The dashed curve in the top panel is the prediction of the shell model [19] re-normalized by a factor of 0.34.

Fig.5. The neutron spectrum produced by the ^{7}Li(p,n)^{7}Be reaction. The peak is at 298 MeV and the distribution extends to ≈240 MeV. The magnitude of the tail is ≈1% of the peak area per MeV.

Fig.6. Typical angular distributions for the ^{54}Fe(n,p)^{54}Mn reaction. The panels are labeled by excitation energy. The distributions from top to bottom are

dominated by ΔL=0,1,2 respectively.The dashed curve is the ΔL=0 fraction of the cross section while the dash-dotted and dotted curve correspond to ΔL=1, and 2 respectively. The full curve is the total fit to the data.

Fig.7. ΔL=0 fitting coefficients for both reactions. Note that the coefficients vary smoothly even though they are determined independently for each energy bin.

Fig.8. Multipole decomposition of the ^{54}Fe(n,p), 1.8° cross section. The ΔL=0 strength was integrated to 10 MeV above which the ΔL=1 strength dominates. The cross-hatched region which dominates the spectrum at $E_x \leq 8$ MeV is the ΔL=0 component. The right-hatched region which peaks around 15 MeV is the ΔL=1 component, while the remaining left-hatched region is the ΔL=2 component.

Fig.9. Multipole decomposition of the ^{54}Fe(p,n), 0° cross section. The ΔL=0 strength was integrated to 15 MeV above which the ΔL=1 strength dominates. Note that the peak at ≈1 MeV has a contribution from the Fermi transition to the IAR. The meaning of the hatching is the same as for fig.8.

Fig.10. Comparison of the ΔL=0 cross section for both reactions with the predictions of the quasi-particle RPA model for B(GT) [23].

Fig.11. Large momentum transfer ^{54}Fe(n,p) spectra compared to the semi-infinite slab model. The dashed curve is the free response while the dotted curve is the 1p-1h RPA response. The full curve includes 2p-2h correlations which redistribute the strength to higher excitation energy.

Fig.12. Comparison of the ^{54}Fe(p,n) cross section with the slab model. For an explanation of the curves, see fig. 11.

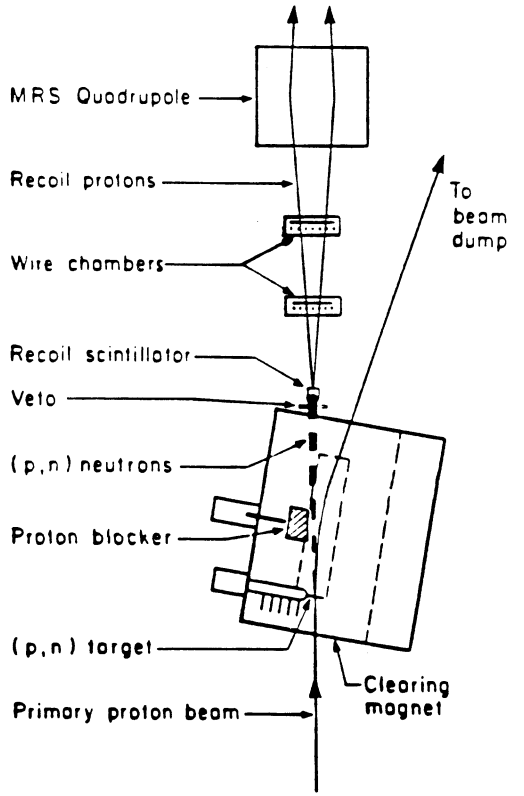

Fig. 1

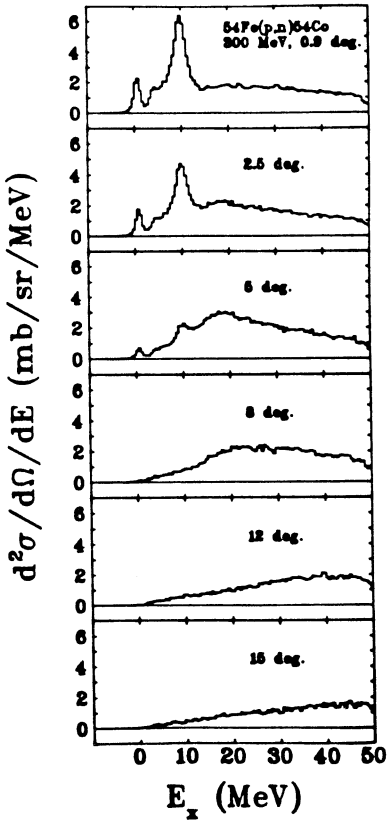

Fig. 2.

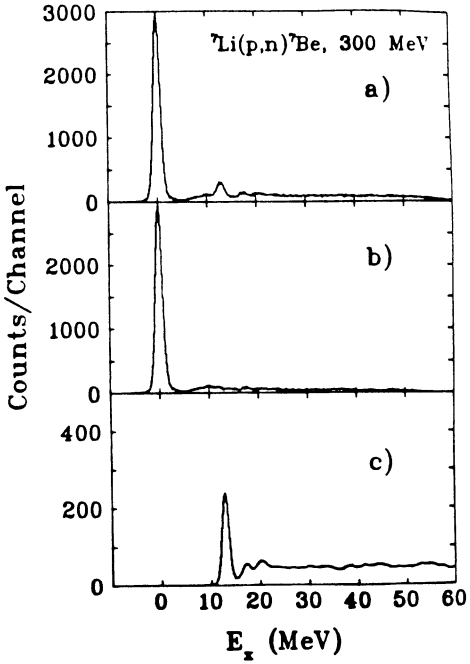

Fig. 3.

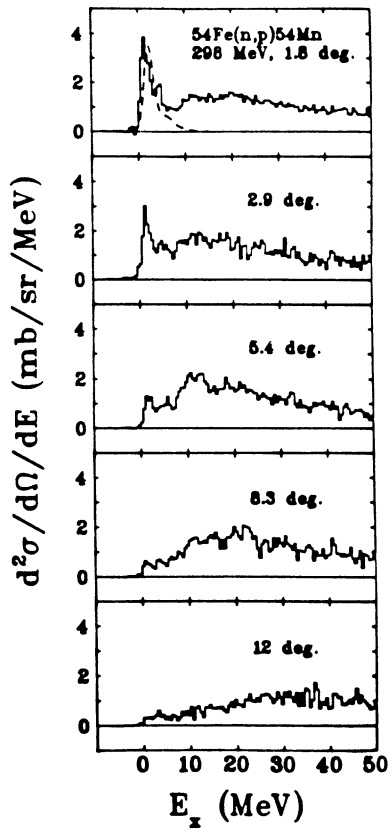

Fig. 4

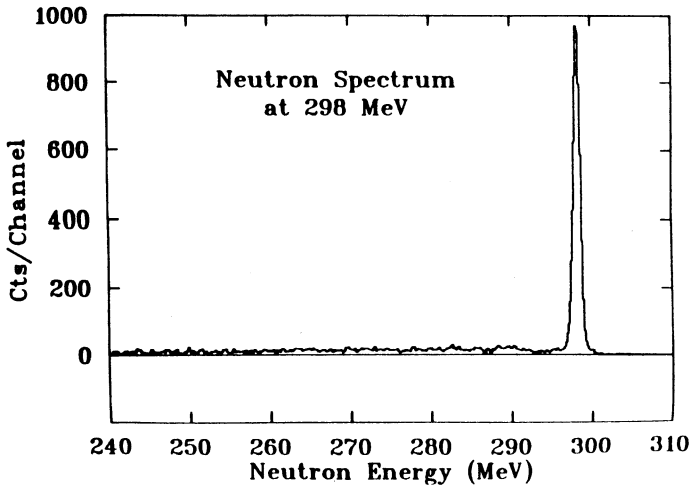

Fig. 5

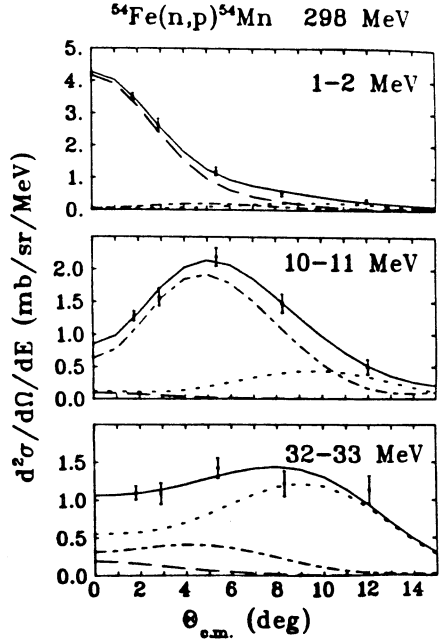

Fig. 6

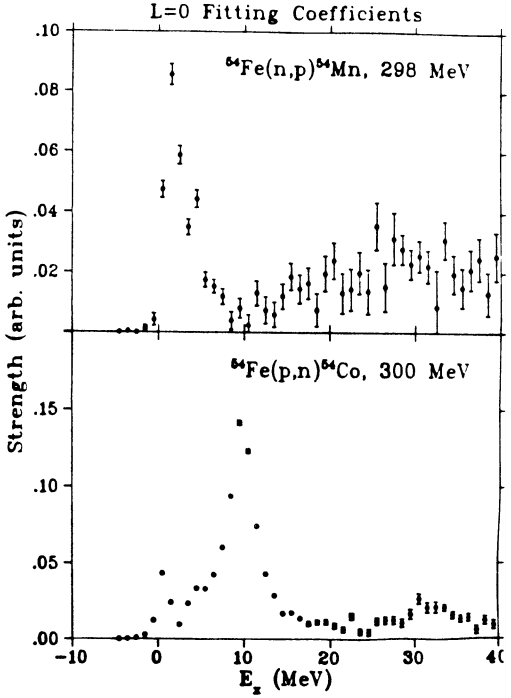

Fig. 7.

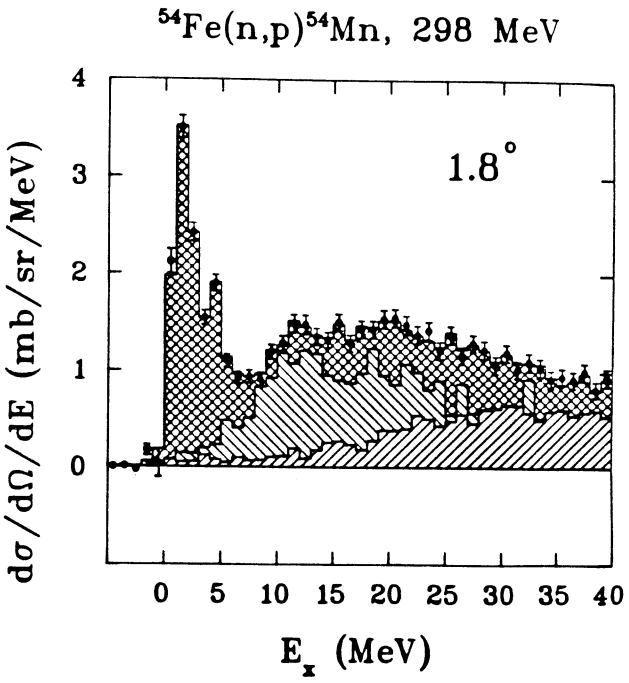

Fig. 8.

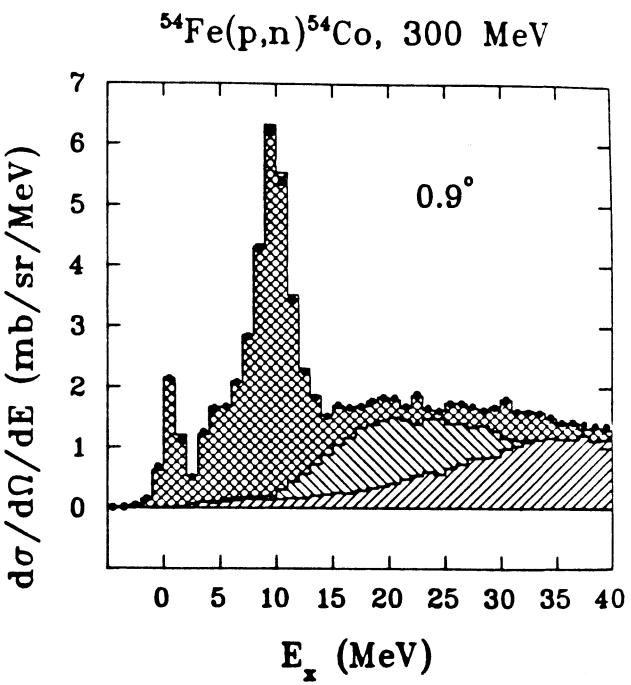

Fig. 9.

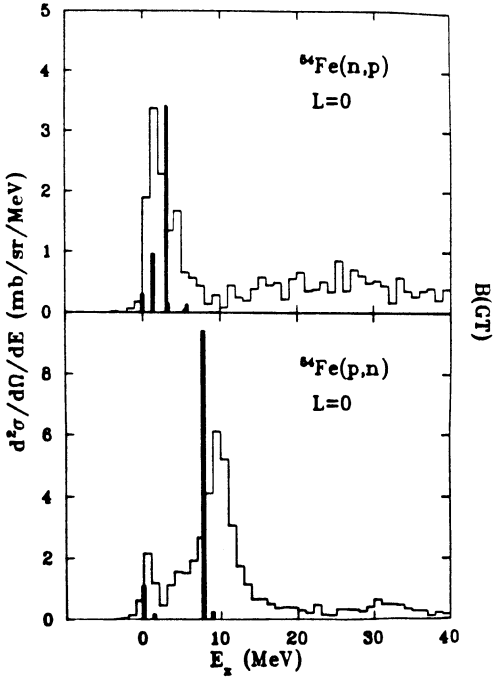

Fig. 10

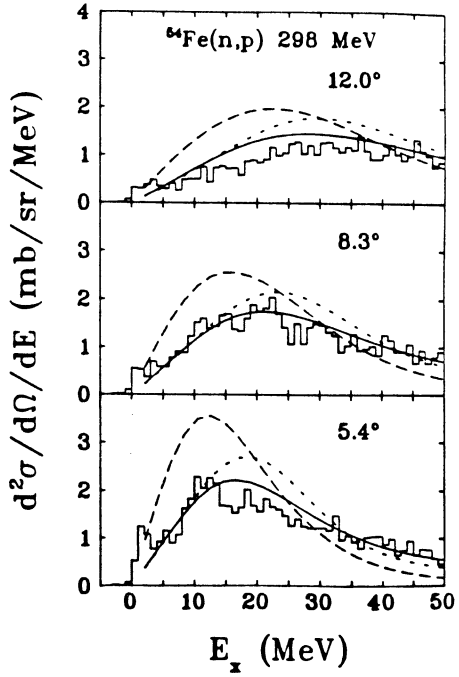

Fig. 11

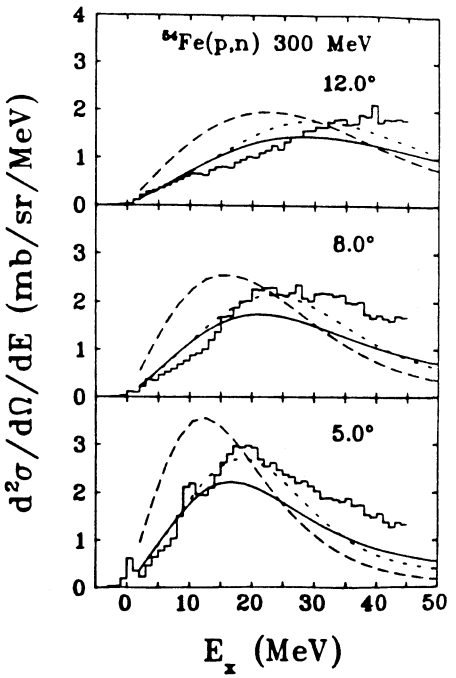

Fig. 12